Catalysis Science & Technology

PAPER

View Article Online
View Journal | View Issue

Cite this: *Catal. Sci. Technol.*, 2014, 4, 688

Verifying the dominant catalytic cycle of the methanol-to-hydrocarbon conversion over SAPO-41

Xin Wang,[a] Weili Dai,[a] Guangjun Wu,[a] Landong Li,*[a] Naijia Guan[a] and Michael Hunger*[b]

Received 29th September 2013,
Accepted 21st November 2013

DOI: 10.1039/c3cy00740e

www.rsc.org/catalysis

In the present work, the mechanism of the methanol-to-hydrocarbon (MTH) conversion over the silicoaluminophosphate SAPO-41 with one-dimensional 10-ring pores has been investigated. For this purpose, catalytic experiments with co-feeding of reactants, *in situ* FTIR and UV/Vis spectroscopy, and ^{1}H MAS NMR spectroscopy of used catalysts upon loading of ammonia were performed. Using these methods, only a low content of aromatics could be observed on the working SAPO-41 catalyst. These findings and the characteristic changes in the ethene selectivity during the co-feeding experiments indicate that alkylaromatics can be excluded as active hydrocarbon pool compounds on SAPO-41 applied as MTH catalysts. On the other hand, dienes and enylic carbenium ions were detected using FTIR and UV/Vis spectroscopy and the formation of amines by reaction of alkenes with ammonia was detected *via* ^{1}H MAS NMR spectroscopy. These results are experimental evidence that large olefins partially existing in their carbenium state dominate the catalytically active hydrocarbon pool on the working SAPO-41. Due to this dominant alkene-based reaction mechanism and the limited formation of aromatics, SAPO-41 is a suitable catalyst for the C_3+C_4 olefin as well as gasoline production.

1. Introduction

Since the world oil reserves are declining, the utilization of alternative feedstocks for the production of petrochemicals is attracting more and more interest. Methanol can be easily produced from synthesis gas obtained by gasification of coal or other sustainable feedstocks. One of the most important routes for methanol conversion is the methanol-to-hydrocarbon (MTH) reaction on microporous catalysts with high or moderate acid strength. This is an oil-free process to obtain hydrocarbons which has drawn significant attention since it was disclosed in the 1970s.[1–4] A variety of microporous catalysts have been explored for MTH conversion.[5–13] Amongst these catalysts, the silicoaluminophosphate SAPO-34 and aluminosilicate-type H-ZSM-5 zeolites have already been commercialized for the methanol-to-olefin (MTO) and methanol-to-gasoline (MTG) conversion, respectively.

The MTH conversion is known as an extremely complex reaction and the understanding of the mechanisms is a great challenge. In the past decades, the origin of the first C–C bond and the detailed reaction mechanism of MTH conversion were the topics of numerous controversy debates.[2,4] The generally discussed routes are based on the formation of a hydrocarbon pool occluded in the cages or pores of the catalysts, to which methanol and dimethyl ether (DME) are added and from which alkenes are split in closed cycles.[14–16] For SAPO-34, an aromatic-based hydrocarbon pool mechanism is widely accepted for the MTH conversion.[17–19] In the case of H-ZSM-5, a similar mechanism involving methylation and subsequent cracking of higher alkenes is proposed in parallel with the aromatic-based hydrocarbon pool mechanism, *i.e.* the dual-cycle mechanism shown in Scheme 1.[7,20–22] This dual-cycle mechanism has significantly improved the general understanding of the catalytic properties of microporous catalysts with different pore architectures and of specific catalysts as a function of time-on-stream (TOS).

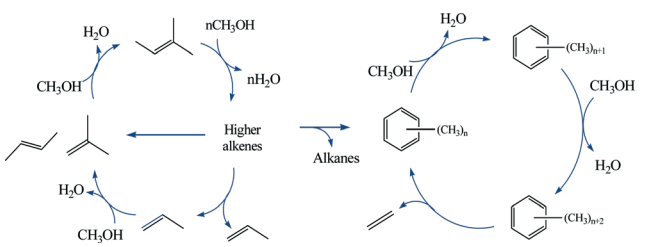

Scheme 1 Concept of the dual-cycle mechanism for the conversion of methanol-to-hydrocarbons over H-ZSM-5, adapted from ref. 4.

[a] *Key Laboratory of Advanced Energy Materials Chemistry (Ministry of Education), College of Chemistry, Nankai University, Tianjin 300071, PR China. E-mail: lild@nankai.edu.cn; Fax: +86 22 23500341; Tel: +86 22 23500341*
[b] *Institute of Chemical Technology, University of Stuttgart, 70550 Stuttgart, Germany. E-mail: michael.hunger@itc.uni-stuttgart.de; Fax: +49-711-685-64081*

Accordingly, the topology of the microporous catalysts significantly influences the reaction intermediates and the reaction mechanism. In SAPO-34 and H-Beta containing cages and crossing intersections (crossing 12-ring pores with diameters of 0.66 nm × 0.67 nm and 0.56 nm × 0.56 nm),[23] respectively, hexamethylbenzene is formed and its further methylated cation, *i.e.* the heptamethylbenzenium cation (heptaMB$^+$) is found to be the dominating intermediate in the formation of light alkenes.[7,17] For H-ZSM-5 possessing crossing intersections of 10-ring pores with diameters of 0.56 nm × 0.53 nm and 0.55 nm × 0.51 nm,[23] lighter polymethylbenzenes (such as xylene, triMB, and tetraMB) are proven to be the main aromatic-based hydrocarbon pool species.[7] On the other hand, for ZSM-22 characterized by one-dimensional 10-ring pores having a diameter of 0.57 nm × 0.46 nm, the aromatic-based hydrocarbon pool mechanism is inhibited, olefin chains grow *via* step by step carbon addition, and the product mixture is rich in higher alkenes.[24] Hence, cages, crossing intersections or large pores are necessary to accommodate polymethylbenzenes (polyMBs), and the size of the pores influences the specific polyMB species, wherein narrow pores support the alkene-based mechanism.

On the other hand, the acid strength of the catalyst also greatly influences the reaction mechanism of the MTH conversion. It has been reported that the primary dehydration reaction and oligomerization of lower olefins requires moderate acid sites, while the aromatization requires strong acid sites.[25] For example, the dual-cycle mechanism is also present in SAPO-5 characterized by large one-dimensional 12-ring pores with a diameter of 0.73 nm × 0.73 nm, but the lower acid strength compared to HZSM-5 shifts the reaction mechanism to the alkene-mediated cycle.[26]

In previous studies, the silicoaluminophosphate SAPO-41, characterized by narrow one-dimensional 10-ring pores with a diameter of 0.70 nm × 0.43 nm and a moderate Brønsted acidity, has been proven to be a suitable MTH catalyst.[11] The present work focuses on the mechanism of the MTH conversion over SAPO-41, and the obtained results are discussed in comparison with those of SAPO-34 studied earlier.[27] Both microporous silicoaluminophosphates, SAPO-41 and SAPO-34, are characterized by Brønsted sites with moderate acid strength. In contrast to SAPO-34 that contains chabazite cages, which are large enough for the formation of polyalkylaromatics and polycyclic aromatics, SAPO-41 has neither cages nor crossing intersections. Therefore, SAPO-41 is an interesting model catalyst for clarifying the effect of its pore architecture on the reaction mechanism and the nature of the hydrocarbon pool compounds responsible for the MTH conversion property of this material.

2. Experimental

2.1 Sample preparation

SAPO-41 was synthesized *via* the hydrothermal route following the procedure described in literature.[28] The chemical composition of the synthetic mixture of SAPO-41 is $1.2Al_2O_3 : H_3PO_3 : 2H_3PO_4 : 4DPA : 0.15SiO_2 : 50H_2O$. The synthesis mixture was hydrothermally treated in a Teflon-lined stainless-steel autoclave at 200 °C for 4 days. After crystallization, the solid phase was separated by centrifugation, washed several times with deionized water and subsequently dried at 80 °C for 12 h. The as-synthesized sample was calcined in flowing synthetic air at 600 °C for 6 h.

2.2 Sample characterization

The X-ray diffraction (XRD) pattern of the sample was recorded on a Bruker D8 diffractometer using CuKα radiation (λ = 1.5418 Å) from 5–50° with a scan speed of $2\theta = 6.0°$ min^{-1}.

A HITACHI S-4700 Scanning Electron Microscope (SEM) was used to study the morphology of the SAPO-41 particles.

The chemical composition of the calcined sample was determined using inductively coupled plasma atomic emission spectroscopy (ICP-AES, IRIS Advantage). The surface area of the calcined sample was determined by means of nitrogen adsorption at −196 °C on a Quantachrome iQ-MP gas adsorption analyzer. Before the nitrogen adsorption, the sample was dehydrated at 200 °C for 2 h. The total surface area was calculated using the Brunauer–Emmett–Teller (BET) equation.

The temperature-programmed desorption of ammonia (NH_3-TPD) was carried out in a quartz U-shaped reactor and monitored using an online chemisorption analyzer (Quantachrome ChemBet 3000). The sample with a mass of *ca.* 0.1 g was pretreated at 600 °C for 1 h in flowing He (30 ml min^{-1}), cooled to 100 °C, and then saturated with 5% NH_3/He. After purging with He for 30 min to eliminate the physically adsorbed ammonia, the NH_3-TPD measurement was performed in flowing He (30 ml min^{-1}) at 100 to 600 °C with a heating rate of 10 °C min^{-1}.

Solid-state NMR experiments were performed on a Bruker Avance III spectrometer at resonance frequencies of 400.1, 104.3, 79.5, and 161.9 MHz for ^{1}H, ^{27}Al, ^{29}Si, and ^{31}P, respectively. The experimental conditions are as follows: single pulse excitation of $\pi/2$ for ^{1}H and ^{31}P, $\pi/6$ for ^{27}Al, and $\pi/4$ for ^{29}Si, with repetition times of 20 s for ^{1}H and ^{29}Si, 0.5 s for ^{27}Al, and 30 s for ^{31}P MAS NMR spectroscopy. The ^{1}H, ^{27}Al, and ^{31}P MAS NMR spectra were recorded with a sample spinning rate of 8 kHz, while the ^{29}Si MAS NMR spectra were obtained at 4 kHz. The ^{27}Al, ^{29}Si, and ^{31}P MAS NMR measurements were performed using hydrated samples. To avoid damage of the silicoaluminophosphate framework by long term hydrolysis, the sample material was exposed to an atmosphere that was saturated with vapours of a $Ca(NO_3)_2$ solution at ambient temperature to be fully hydrated one day before the NMR investigations. Before the ^{1}H MAS NMR studies of the fresh SAPO-41 sample (TOS = 0 min), the sample was dehydrated at 450 °C at a pressure below 10^{-2} Pa for 12 h. After dehydration, the sample was sealed and kept in glass tubes before being filled into the MAS NMR rotor in a glove box purged with dry nitrogen gas. The sample treatment utilized in the case of ^{1}H MAS NMR investigations on used MTH

catalysts is described in section 2.5. Quantitative ^{1}H MAS NMR measurements were performed by a comparison of the signal intensities of the samples under study with that of an external standard (dehydrated zeolite H,Na-Y with an ion exchange degree of 35%). The decomposition and simulation of NMR spectra were carried out using the Bruker software WINNMR and WINFIT.

2.3 Catalytic investigations

The MTH reaction was performed in a fixed-bed reactor at atmospheric pressure. Typically, 0.4 g of the sample (sieve fraction, 0.25–0.5 mm) was placed in a stainless steel reactor (5 mm i.d.) and activated under flowing N_2 at 450 °C for 0.5 h, after which the temperature was decreased to the desired temperature. Pure methanol or methanol with a co-feeding agent was pumped in at 0.5 mL h^{-1}, corresponding to the weight hourly space velocity (WHSV) of 1 h^{-1}. The products were analyzed using an online gas chromatograph equipped with a flame ionization detector and a capillary column DB-624 to separate the products. The temperature of the column was maintained at 40 °C for 7 min and then increased to 200 °C at a ramping rate of 10 °C min^{-1} and maintained at 200 °C for 4 min.

2.4 *In situ* UV/Vis and FTIR studies of the MTH conversion on SAPO-41

The nature of organic compounds formed on the catalysts during the MTH reaction was *in situ* monitored by FTIR and UV/Vis spectroscopy. FTIR spectra were recorded in diffuse reflection mode on a Bruker Tensor 27 spectrometer equipped with a liquid N_2 cooled high sensitivity MCT detector and an *in situ* reaction chamber. The catalyst samples weighing *ca.* 20 mg were finely ground and placed in the chamber. Prior to each experiment, the samples were activated in flowing He at 450 °C for 1 h and cooled to 400 °C to record the background spectrum. Then, methanol was fed into the chamber at 0.025 mL h^{-1} (WHSV = 1.0 h^{-1}) and the time-resolved spectra were recorded with a resolution of 4 cm^{-1} and an accumulation of 128 scans.

Diffuse reflectance UV/Vis spectra were recorded using an AvaSpec-2048 fiber optic spectrometer with an AvaLight-DH-S deuterium light source manufactured by Avantes and a glass fiber reflection probe HPSUV1000A manufactured by Oxford Electronics. Before the MTH reaction, the glass fiber reflection probe was placed in the fixed-bed reactor on the top of the catalyst with a gap of *ca.* 1.0 mm. Reference UV/Vis spectra of catalysts were recorded at reaction temperature prior to starting the methanol flow. The *in situ* UV/Vis spectra were recorded in the range of 200–600 nm during the MTH reaction.

2.5 Solid-state ^{1}H NMR characterization of surface sites

The Brønsted acid sites and occluded organic compounds formed on the used MTH catalysts were characterized by means of ^{1}H MAS NMR spectroscopy. For this purpose, a Bruker Avance III 400WB spectrometer at the resonance frequency of 400.1 MHz with $\pi/2$ single pulse excitation, the repetition time of 10 s, and a 2.5 mm MAS NMR probe with the sample spinning rate of 25.0 kHz were used. The MTH reaction performed at 400 °C was quenched by stopping the methanol flow and cooling down to room temperature under flowing nitrogen before taking the catalyst samples. Subsequently, the catalyst samples were transferred from the fixed-bed reactor to MAS NMR rotors without contact with air in a glove box purged with dry nitrogen gas. The determination of the number of accessible Brønsted acid sites was performed by adsorption of ammonia at room temperature. After the ammonia loading, the samples were evacuated at 180 °C for 2 h to eliminate physisorbed ammonia. Quantitative ^{1}H MAS NMR measurements and their evaluation were performed as described in section 2.2.

3. Results and discussion

3.1 Results of the catalyst characterization

The XRD pattern of the as-synthesized SAPO-41 sample in Fig. 1 shows typical diffraction lines corresponding to the AFO structure, which indicate that pure SAPO-41 was obtained.[28] As shown in the SEM image (see inset) of the as-synthesized SAPO-41 material, the particles appear as hexagonal prisms with dimensions of *ca.* 2 μm diameter and *ca.* 6 μm height.

The $n_{Si}/(n_{Si} + n_{Al} + n_P)$ of calcined SAPO-41 determined using ICP-AES is 0.03. The surface area of the calcined sample was determined to be 268 m^2 g^{-1}, indicating the intactness and accessibility of the pore system.

The acidic properties of the activated and fresh SAPO-41 material (TOS = 0 min) were characterized by NH_3-TPD (Fig. 2). The obtained curve consists of a low-temperature ammonia desorption peak centered at 210 °C attributed to weak acid sites and a medium-temperature ammonia desorption peak centered at 320 °C assigned to moderate acid sites. According to earlier studies of Meriaudeau *et al.*,[29] this NH_3-TPD curve is typical for SAPO-41 and most of the other pure SAPO materials.

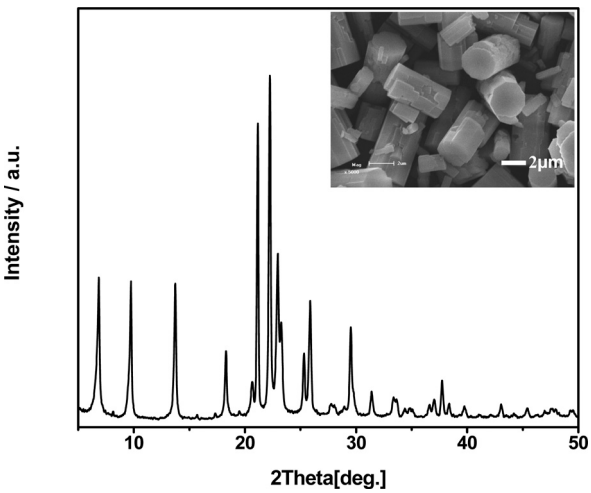

Fig. 1 XRD pattern and SEM image of the as-synthesized SAPO-41 material.

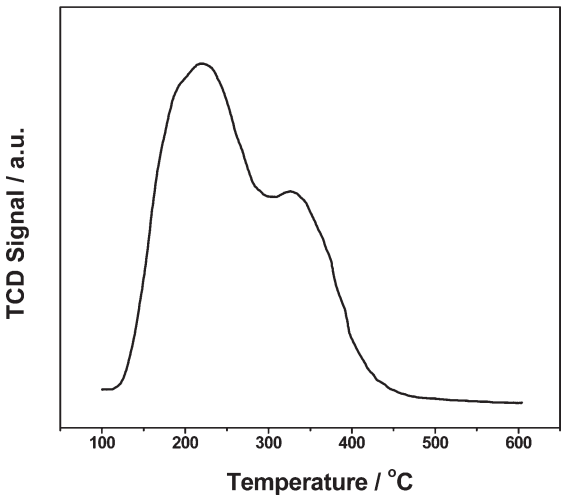

Fig. 2 NH_3-TPD profile of the calcined SAPO-41 material.

For a better understanding of the acidic and textural properties of SAPO-41 after calcination, multi-nuclear solid-state NMR spectroscopy was employed to analyze the Brønsted acid sites and the bonding states of silicon, phosphorus and aluminum in the SAPO-41 framework (Fig. 3). The signals occurring at 3.6 and *ca.* 4.7 ppm in the ^{1}H MAS NMR spectrum of the calcined and dehydrated material, both accompanied by spinning sidebands with similar relative intensities (not shown), are due to bridging OH groups (Si(OH)Al) acting as Brønsted acid sites. Specifically, signals at 3.6 ppm indicate the presence of non-interacting Si(OH)Al groups in pores and cages, while ^{1}H MAS NMR signals at 4.7 ppm are assigned to Si(OH)Al groups involved in interactions with neighboring framework oxygen atoms, such as in small structural building units.[30] The weak ^{1}H MAS NMR signals at 1.6 and 2.6 ppm are generally explained by hydroxyl groups at the outer crystal surface and framework defect sites, *i.e.* by SiOH, AlOH and POH groups.[31] The ^{27}Al MAS NMR signal at 38 ppm in the spectrum of the calcined and rehydrated SAPO-41 material is assigned to tetrahedrally coordinated framework aluminum atoms, while the signal at −14 ppm is due to octahedrally coordinated aluminum atoms formed through a reversible coordination of two water molecules to tetrahedrally coordinated framework aluminum atoms or caused by extra-framework aluminum species.[30] The signal at −30 ppm in the ^{31}P MAS NMR spectrum is due to tetrahedrally coordinated phosphorus atoms in the aluminophosphate regions of the SAPO framework.[30] The narrow ^{29}Si MAS NMR signal at −90 ppm indicates incorporation of silicon atoms on tetrahedral framework positions with four neighboring aluminum atoms at T positions.[30] The ^{29}Si MAS NMR spectrum is clear evidence that most of the silicon atoms are incorporated into the SAPO-41 framework in a highly isolated manner since no ^{29}Si MAS NMR signals of silicon islands (*ca.* −110 ppm) occurred. This leads to the formation of a corresponding number of bridging OH groups. The above-mentioned results of the solid-state NMR characterization indicate that the SAPO-41 material under study maintains its Brønsted acid sites and good textural properties after calcination.

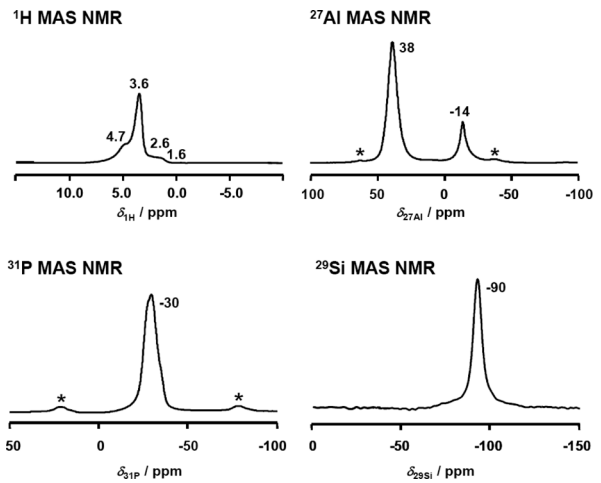

Fig. 3 ^{1}H, ^{27}Al, ^{29}Si, and ^{31}P MAS NMR spectra of the calcined SAPO-41 material recorded in the dehydrated state (^{1}H) and upon rehydration (^{27}Al, ^{29}Si, and ^{31}P). Asterisks indicate spinning sidebands.

3.2 Catalytic investigation of SAPO-41 applied in the MTH conversion

Fig. 4 shows the time-on-stream (TOS) behavior of the methanol conversion and product selectivity of the SAPO-41 catalyst at reaction temperatures of 350 to 450 °C. At 350 °C, 100% methanol conversion is maintained up to TOS = 4 h, and then gradually decreased to 70% at TOS = 16 h. With the progress of the MTH reaction, the selectivity to C_2–C_4 olefins gradually decreased and dropped from the initial 50 to 25% at TOS = 16 h. With increasing reaction temperature up to 450 °C, 100% methanol conversion could be kept for more than 16 h, and the initial selectivity to C_2–C_4 olefins was increased to 75%. These findings and the formation of methane can be explained by an increasing tendency toward cracking of heavier hydrocarbons to lighter fragments at high temperatures.[32] In addition, the selectivity to aromatics (mainly polymethylbenzenes, *e.g.* toluene, xylene, and durene) decreases obviously with increasing reaction temperature. This may be additional support for an increased tendency toward cracking of large organic compounds. On the other hand, oligomers desorb from the catalyst before they can form aromatics at high reaction temperatures.[33] Both these assumptions are in line with the longer lifetime of the SAPO-41 catalyst at 450 °C observed in comparison with its catalytic properties at 350 °C. Moreover, we could not exclude the possibility that the longer lifetime is simply due to the higher reaction rates at higher temperatures, as suggested by Olsbye *et al.* from kinetic modelling.[34] Interestingly, more than 50% of the gasoline-range hydrocarbons (C_5–C_8 alkanes and alkenes) can be obtained over the SAPO-41 catalyst at the relatively low reaction temperature of 400 °C. From this point of view, SAPO-41 can be applied as an eligible catalyst for the gasoline production *via* the environment-friendly MTH process.

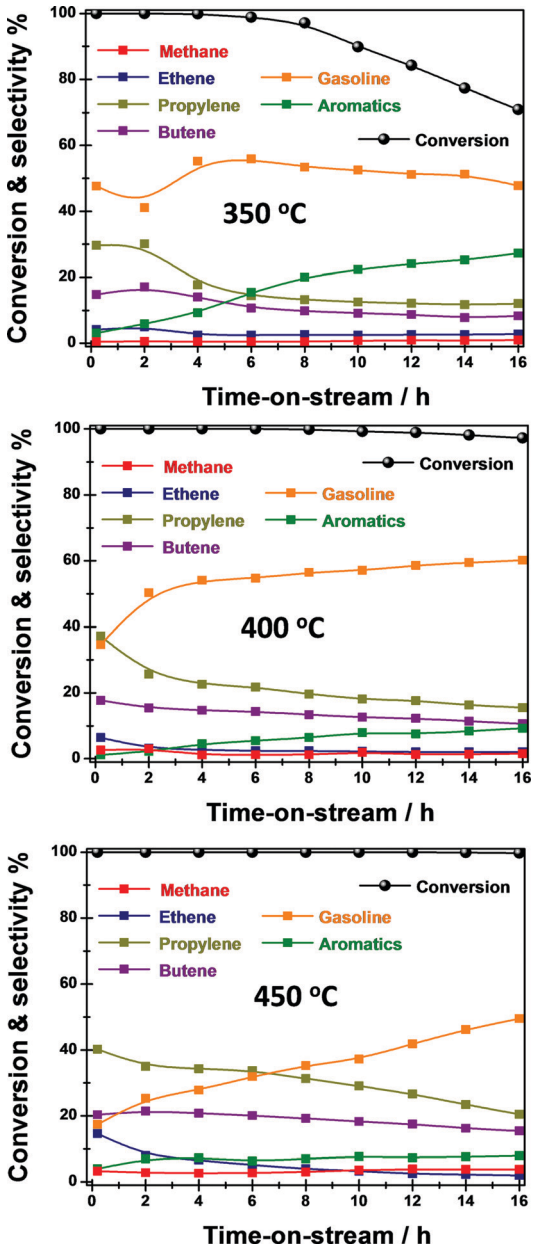

Fig. 4 Methanol conversion and product selectivity during the MTH reaction on SAPO-41 at different reaction temperatures.

3.3 *In situ* UV/Vis and FTIR studies of organic compounds formed on SAPO-41 by the MTH conversion

The nature of organic compounds formed during the MTH conversion on SAPO-41 was monitored using *in situ* UV/Vis and FTIR spectroscopy. Fig. 5 shows the UV/Vis spectra of the species formed on SAPO-41 under steady-state conditions at 400 °C with TOS up to 180 min. After TOS = 20 min, bands at 280, 370 and 440 nm occur, while for further increased TOS, an additional band at 240 nm is formed with a slightly lower intensity compared with the band at 280 nm. With the progress of the MTH reaction, the band at 370 nm is more and more overlapped with the band at 440 nm. Generally, the bands at 240 and 280 nm are assigned to dienes and

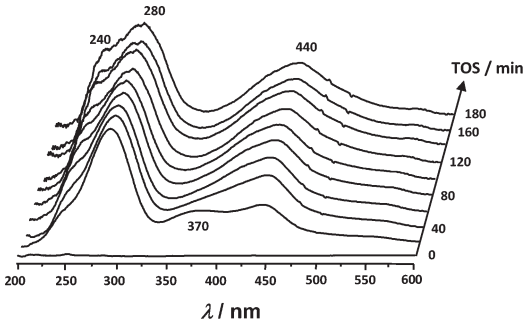

Fig. 5 *In situ* UV/Vis spectra recorded during the MTH reaction on SAPO-41 at 400 °C.

aromatics, respectively.[35] The bands at 370 and 440 nm may hint at the formation of dienylic and trienylic carbenium ions, respectively,[35] or different polycyclic aromatics.[36]

For SAPO-34 applied as MTO catalysts, a strong UV/Vis band was observed in the spectral range of 350 to 450 nm, which strongly increased with increasing TOS.[27] For SAPO-34, however, this band occurs at 400 nm and is significantly narrower than those at 370 and 440 nm in the case of SAPO-41. The band at 400 nm in the UV/Vis spectra of working SAPO-34 was assigned to polycyclic aromatics, which agrees well with the formation of aromatic compounds in the chabazite cages of this silicoaluminophosphate. Considering the different spectral properties of the UV/Vis band at 400 nm for SAPO-34 and those of the bands at 370 and 440 nm for SAPO-41, the latter bands are explained by the presence of polyenylic carbenium ions.

In Fig. 6, the *in situ* FTIR spectra recorded during the MTH conversion over SAPO-41 performed at 400 °C and recorded up to TOS = 180 min are shown. The weak bands of C–H stretching vibrations occurring in the range of 2825–2955 cm^{-1} are difficult to assign to specific organic compounds, while the weak bands at 1345 and 1460 cm^{-1} are typical for skeletal C=C vibrations of aromatics and bending vibrations of the C–H bond.[37] The intensities of these bands that slightly increase with the progress of the MTH reaction, however, are weak in comparison with those observed in the same spectral ranges in *in situ* FTIR studies of SAPO-34 applied as MTO catalysts.[27] The most intensive and characteristic

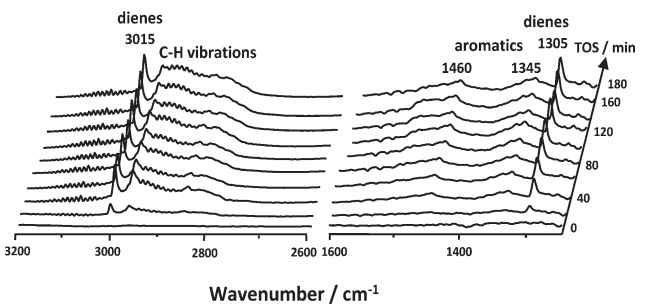

Fig. 6 *In situ* FTIR spectra recorded during the MTH reaction on SAPO-41 at 400 °C.

FTIR bands observed for working SAPO-41 are those appearing at 3015 and 1305 cm^{-1}, which are due to the C–H stretching and methyl bending vibrations of dienes.[38] The intensities of these bands strongly increase during the first minutes of the MTH reaction and are stable during the further progress of the MTH conversion indicating continuous formation of dienes on SAPO-41. This finding agrees well with the observed properties of the UV/Vis band of dienes at 240 nm (Fig. 5).

3.4 Solid-state NMR studies of surface sites and organic compounds on SAPO-41

In order to investigate the fate of Brønsted acid sites as a function of the reaction time, samples of the SAPO-41 catalyst were taken after TOS = 0 to 240 min. These samples were investigated using ^{1}H MAS NMR spectroscopy without and after loading of ammonia (Fig. 7, left and right, respectively). The ^{1}H MAS NMR spectra of the SAPO-41 catalysts shown on the left-hand side of Fig. 7 consist of the signals of bridging hydroxyl groups Si(OH)Al at 3.6 and *ca.* 4.7 ppm already discussed in section 3.1. With increasing TOS, additional signals of organic compounds occur in the aliphatic region at *ca.* 0 to 2 ppm and in the olefinic and aromatic region at *ca.* 5 to 7 ppm. These spectral ranges are also typical for non-branched and branched dienes, such as 2,4-hexadiene (δ_{1H} = 1.7 ppm and 5.5 to 5.9 ppm),[39] 2,3-dimethyl-1,3-butadiene (δ_{1H} = 1.9 ppm and 4.9 to 5.0 ppm)[39] *etc.*, which supports the assignment of dienes in the *in situ* FTIR spectra shown in Fig. 6.

The weak signals appearing at 0.2 ppm in the ^{1}H MAS NMR spectra of the SAPO-41 materials used as MTO catalysts (TOS = 30 to 240 min) indicate the formation of a few AlOH groups probably formed by the reaction of water and framework aluminum species.[31] Typically, these signals are characterized by weak spinning sidebands (not shown). Similarly, the weak signals at 3.9 to 4.0 ppm are also due to surface POH groups formed from the hydrolysis of –Al–O–P– bonds in the SAPO-41 framework. The assignment of these POH groups is supported by FTIR studies of SAPO-41 conducted by Meriaudeau *et al.*[29] These authors observed bands of POH stretching vibrations at 3677 cm^{-1} near the band of bridging OH groups at 3627 cm^{-1}.

For a better quantification of the number of accessible bridging OH groups acting as Brønsted acid sites in SAPO-41 applied as MTH catalysts, ammonia was loaded on the samples leading to the formation of ammonium ions with a chemical shift of 6.8 ppm (Fig. 7, right).[40] Evaluation of the signal intensities at 6.8 ppm gave the densities of accessible Brønsted acid site to be 0.36 to 0.19 mmol g^{-1} for SAPO-41 catalysts applied in the MTH conversion at TOS = 0 to 240 min (Table 1, column 2). For SAPO-34, it was observed that the bridging OH groups are rapidly covered by aromatics and other larger organic species causing a rapid catalyst deactivation due to their blocking.[27] In the case of SAPO-41, the one-dimensional 10-membered ring channels permit the diffusion also of larger alkanes and alkenes as well as aromatics, so that the apparent consumption and blocking of Brønsted acid sites in SAPO-41 are much slower than that found for SAPO-34 used as MTH catalysts. Accordingly, SAPO-41 has a much longer lifetime in the methanol conversion under similar reaction conditions.

Upon loading of the SAPO-41 samples used as MTH catalysts with ammonia, additional ^{1}H MAS NMR signals appeared at 2.8 ppm (Fig. 7, right). The signals hint at the formation of mono-substituted secondary amines by reaction of ammonia with alkenes that are probably in their carbenium state. Possible examples are ethylamine (δ_{1H} = 2.36 ppm), propylamine (δ_{1H} = 2.59 ppm) or secondary NH_2 groups in larger alkane chains (δ_{1H} = 2.50 ppm).[39] It is interesting to note that the amines formed on aromatics and alkylaromatics can be excluded from contributing to the signals at 2.8 ppm due to their significantly higher chemical shifts (*e.g.* δ_{1H} = 3.49 to 3.40 ppm for mono- to pentamethylphenylamine). Also, protonated NH_x groups have much higher chemical shift values than 2.8 ppm.

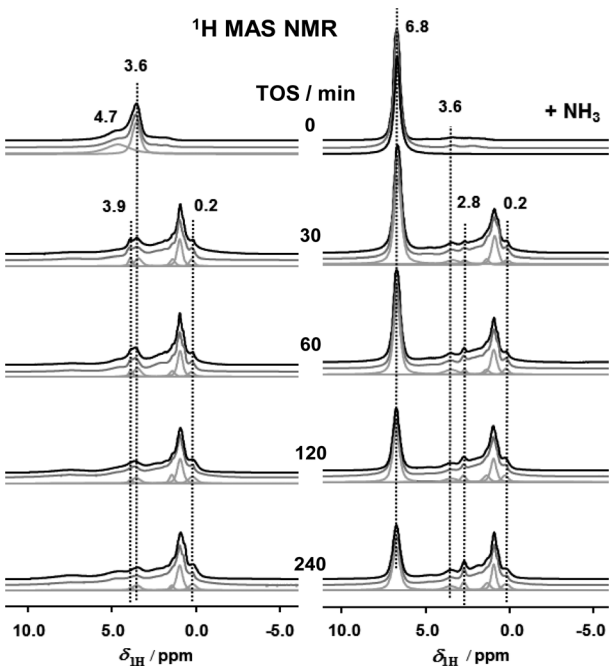

Fig. 7 ^{1}H MAS NMR spectra of SAPO-41 samples used as MTH catalysts at 400 °C and for TOS = 0 to 240 min, recorded before (left) and after ammonia loading (right).

Table 1 Number of accessible Si(OH)Al groups, n_{SiOHAl}, and amines, n_{amine}, formed by reaction of ammonia with reactive organic compounds on calcined SAPO-41 (TOS = 0 min) and on samples used as MTH catalysts at 400 °C for TOS = 30 to 240 min, determined using quantitative ^{1}H MAS NMR spectroscopy

TOS/min	n_{SiOHAl} (mmol g^{-1})	n_{amine} (mmol g^{-1})
0	0.36	0
30	0.30	0.003
60	0.27	0.006
120	0.22	0.009
240	0.19	0.013

The observed amines must be formed already at low temperature (180 °C), which indicates the high reactivity of the organic compounds reacting with the adsorbed ammonia. Probably, these organic compounds are the enylic or polyenylic carbenium ions responsible for the UV/Vis bands occurring at 370 and 440 nm in the *in situ* UV/Vis spectra shown in Fig. 5. Evaluation of the ^{1}H MAS NMR signals at 2.8 ppm gave the number of amine molecules summarized in column 4 of Table 1.

3.5 Co-feeding of aromatics and large alcohols during the MTH conversion

Considering the aromatic-based cycle of the hydrocarbon pool mechanism shown in Scheme 1, right-hand side, toluene or xylene introduced as co-feeds may contribute to the MTH reaction. In this case, they would be responsible for the formation of small reaction products, such as ethene. On the other hand, co-feeding of ethanol and longer-chain alcohols may help to understand the role of olefins in the MTH conversion since these alcohols are rapidly dehydrated to their corresponding olefins. Therefore, co-feeding experiments are interesting tools for clarifying or supporting reaction mechanisms of the MTH conversion under study.

Table 2 shows the results of the co-feeding experiments during MTH conversion over SAPO-41 and the initial activities at TOS = 0.2 h are used for subsequent discussion. Without co-feeding, the SAPO-41 catalyst has a much lower selectivity to ethene (6.4%) in comparison with SAPO-34 (25–30%).[11,27] Already this finding hints at the small contribution of the aromatic-based cycle in the MTH conversion over SAPO-41 (Scheme 1, right-hand side) since this catalytic cycle is responsible for the ethene formation. Upon co-feeding of toluene and xylene, on the other hand, the ethene selectivity is strongly enhanced from 6.4% to about 30%, while the selectivity toward propene and gasoline-range hydrocarbons (C_5–C_8) decreases accordingly. These results indicate that (i) toluene and xylene can act as the hydrocarbon pool species of the MTH conversion over SAPO-41. Without co-feeding of aromatics, however, (ii) a very small number of aromatics is formed in the pores of SAPO-41 to make the aromatic-based cycle the dominating MTH reaction mechanism for this silicoaluminophosphate. Also, co-feeding of ethanol leads to a strong increase in the ethene selectivity from 6.4% without and 32.7% with co-feeding (Table 2). This finding can be explained by direct formation of ethene *via* dehydration of ethanol over silicoaluminophosphates and also at weak Brønsted acid sites near the outer surface of the SAPO-41 particles.[41] Meanwhile, there is a significant decrease in the selectivities to C_5–C_8 in the case of ethanol co-feeding. This finding indicates that the ethene molecules, which are formed by dehydration of ethanol, cannot be converted to higher olefins *via* the methylation route, as supported by the high reaction barrier of 0.79 eV from theoretical calculations.[42] In this case, the ethene formed *via* dehydration of ethanol can rapidly desorb from the catalyst particles and be detected in the reaction outlet.

For co-feeding of isopropanol and 1-butanol, no obvious increase in the corresponding olefin formation could be observed, while a strong increase in C_5–C_8 formation is observed. Since the dehydration of isopropanol and 1-butanol readily takes place in the presence of acid sites, this finding may hint at the further conversion of dehydration product olefins. It has been reported that the reaction barriers for the methylation of propene and butene are 0.35 eV and 0.20 eV,[42] respectively, which are much lower than that of ethene (0.79 eV). Under a reaction temperature of 400 °C, the methylation of C_3+ olefins readily takes place, which results in the increase in C_5–C_8 formation.

Table 2 Product distribution in MTH conversion over SAPO-41 at 400 °C, TOS = 0.2 or 1 h, with different co-feedings of reactants

Co-feeding	TOS (h)	Conc. (v/v%)	Selectivity %				
			$C_2^=$	$C_3^=$	$C_4^=$	C_5–C_8	Aromatics
None	0.2	0	6.4	37.2	17.8	34.9	1.1
	1		4.0	28.6	16.5	42.9	1.7
Ethanol	0.2	16.7	32.7	22.6	14.6	24.1	4.5
	1		31.6	19.5	13.2	26.1	7.8
Isopropanol	0.2	16.7	2.5	28.4	19.0	44.4	4.1
	1		1.4	22.4	18.0	46.9	7.2
1-Butanol	0.2	16.7	2.2	25.1	19.7	47.0	5.4
	1		1.4	21.9	18.6	51.7	5.7
Toluene	0.2	2.0	28.8	22.3	16.8	26.5	4.9
	1		26.9	22.0	15.4	29.2	5.5
Xylene	0.2	2.0	31.2	21.3	15.9	25.2	5.6
	1		29.6	19.8	15.2	28.6	6.4

3.6 Mechanism of the MTH conversion over SAPO-41

Investigations of the MTH conversion on numerous zeolite catalysts performed in the past decades led to the dual-cycle concept (Scheme 1) as the best explanation for the different product selectivities obtained for zeolites with various pore systems and in specific states of their catalyst lifetime and for materials with strong or moderate Brønsted acid sites. The aim of the present study on SAPO-41 was to clarify whether the aromatic- as well as alkene-based catalytic cycles contribute to the MTH conversion or a single catalytic cycle dominates. Furthermore, the variety of possible hydrocarbons contributing to the catalytically active hydrocarbon pool in SAPO-41 had to be limited to *e.g.* a group of similar organic compounds.

A very interesting finding of the catalytic experiments with co-feeding of methylaromatics was the strong increase in the ethene selectivity indicating that methylaromatics in principle can work as active hydrocarbon-pool compounds in SAPO-41. In the case of the conversion of pure methanol over SAPO-41, however, a very low number of aromatics is formed and exists in the SAPO-41 pores during the MTH conversion, leading to the observed low selectivity to ethene. This explanation is supported by *in situ* UV/Vis and FTIR spectroscopy results, hinting at a much lower content of aromatic deposits on SAPO-41 in comparison with SAPO-34. Furthermore, while ^{1}H MAS NMR studies of SAPO-34 applied as MTH catalysts gave evidence for the presence of benzene-based carbenium

ions,[40] these species could not be detected for the SAPO-41 catalysts treated under similar conditions. All these findings indicate that the aromatic-based cycle is not the dominating reaction mechanism of the MTH conversion over SAPO-41.

Already, the high selectivities to propene and butenes as well as the high yield of gasoline (C_5–C_8) in the MTH conversion on SAPO-41 without co-feeding of other reactants hint at a reaction mechanism based on large olefins as active hydrocarbon pool compounds. Support for this explanation was obtained from the detection of dienes and polyenyl carbenium ions during the MTH conversion *via in situ* UV/Vis and FTIR spectroscopy. Interestingly, the adsorption of ammonia on SAPO-41 samples applied as MTH catalysts led to the formation of amines by the reaction of ammonia with alkenes that are probably in their carbenium state, but not with aromatics or with their benzenium ions. Also this finding is an indication that large olefins and not aromatics are the most active organic compounds in SAPO-41.

An important advantage of SAPO-41 is the relative low consumption rate of Brønsted acid sites in comparison with SAPO-34 under identical reaction conditions.[27] This property of SAPO-41 is due to the absence of pore blocking by aromatic deposits, improving the reactant diffusion and desorption also for large reaction products, such as gasoline compounds (C_5–C_8) and aromatics.

4. Conclusion

By means of catalytic investigations of the MTH conversion over SAPO-41 without and with co-feeding of aromatics and large alcohols, *in situ* UV/Vis and FTIR spectroscopy, and ^{1}H MAS NMR spectroscopy of used catalyst samples upon loading of ammonia, the dominant catalytic cycle of the methanol conversion was investigated. Interestingly, a strong increase in the ethene selectivity was observed during co-feeding of methylaromatics (toluene, xylene) indicating that ethene formation according to the aromatic-based pathway (Scheme 1, right-hand side) is in principle possible in the narrow 10-ring pores of SAPO-41. However, the low ethene selectivity obtained for the conversion of pure methanol as well as the bands of aromatic deposits detected using UV/Vis and FTIR spectroscopy hint to a low content of aromatics on SAPO-41 under steady state conditions of the MTH conversion. All these findings led to an exclusion of the aromatic-based cycle as the dominant mechanism of the MTH conversion over SAPO-41.

On the other hand, *in situ* UV/Vis and FTIR spectroscopy evidenced the presence of dienes and polyenylic carbenium ions on SAPO-41 under reaction conditions. Furthermore, ^{1}H MAS NMR investigations of SAPO-41 samples applied as MTH catalysts and loaded with ammonia indicated the formation of amines with alkenes probably in their carbenium state, but not with aromatics or benzenium ions. Also these observations support the presence of large olefins, which are the active hydrocarbon pool compounds of the MTH conversion over SAPO-41 and make the alkene-based cycle (Scheme 1, left-hand side) the dominating mechanism.

Acknowledgements

This work was supported by the National Natural Science Foundation of China (21303089), 111 Project (B12015), the Ministry of Education of China (NCET-11-0251) and the Collaborative Innovation Center of Chemical Science and Engineering (Tianjin). Furthermore, M.H. wants to acknowledge the financial support of Deutsche Forschungsgemeinschaft.

References

1 C. D. Chang, *Catal. Rev. Sci. Eng.*, 1983, **25**, 1–118.
2 M. Stöker, *Microporous Mesoporous Mater.*, 1999, **29**, 3–48.
3 J. F. Haw, W. G. Song, D. M. Marcus and J. B. Nicholas, *Acc. Chem. Res.*, 2003, **36**, 317–326.
4 U. Olsbye, S. Svelle, M. Bjørgen, P. Beato, T. V. W. Janssens, F. Joensen, S. Bordiga and K. P. Lillerud, *Angew. Chem., Int. Ed.*, 2012, **51**, 2–24.
5 A. T. Aguayo, A. G. Gayubo, R. Vivanco, M. Olazar and J. Bilbao, *Appl. Catal., A*, 2005, **283**, 197–207.
6 A. G. Gayubo, A. T. Aguayo, A. Alonso, A. Atutxa and J. Bilbao, *Catal. Today*, 2005, **106**, 112–117.
7 S. Svelle, U. Olsbye, F. Joensen and M. Bjørgen, *J. Phys. Chem. C*, 2007, **111**, 17981–17984.
8 M. Castro, S. J. Warrender, P. A. Wright, D. C. Apperley, Y. Belmabkhout, G. Pirngruber, H. K. Min, M. B. Park and S. B. Hong, *J. Phys. Chem. C*, 2009, **113**, 15731–15741.
9 J. W. Park, S. J. Kim, M. Seo, S. Y. Kim, Y. Sugi and G. Seo, *Appl. Catal., A*, 2008, **349**, 76–85.
10 J. H. Lee, M. B. Park, J. K. Lee, H. K. Min, M. K. Song and S. B. Hong, *J. Am. Chem. Soc.*, 2010, **132**, 12971–12982.
11 W. Dai, X. Wang, G. Wu, N. Guan, M. Hunger and L. Li, *ACS Catal.*, 2011, **1**, 292–299.
12 M. A. Djieugoue, A. M. Prakash and L. Kevan, *J. Phys. Chem. B*, 2000, **104**, 6452–6461.
13 S. Teketel, W. Skistad, S. Benard, U. Olsbye, K. P. Lillerud, P. Beato and S. Svelle, *ACS Catal.*, 2012, **2**, 26–37.
14 I. M. Dahl and S. Kolboe, *Catal. Lett.*, 1993, **20**, 329–336.
15 I. M. Dahl and S. Kolboe, *J. Catal.*, 1994, **149**, 458–464.
16 I. M. Dahl and S. Kolboe, *J. Catal.*, 1996, **161**, 304–309.
17 B. Arstad and S. Kolboe, *J. Am. Chem. Soc.*, 2001, **123**, 8137–8138.
18 B. Arstad and S. Kolboe, *Catal. Lett.*, 2001, **71**, 209–212.
19 W. G. Song, J. F. Haw, J. B. Nicholas and C. S. Heneghan, *J. Am. Chem. Soc.*, 2000, **122**, 10726–10727.
20 S. Svelle, F. Joensen, J. Nerlov, U. Olsbye, K. P. Lillerud, S. Kolboe and M. Bjørgen, *J. Am. Chem. Soc.*, 2006, **128**, 14770–14771.
21 M. Bjørgen, S. Svelle, F. Joensen, J. Nerlov, S. Kolboe, F. Bonino, L. Palumbo, S. Bordiga and U. Olsbye, *J. Catal.*, 2007, **249**, 195–207.
22 S. Llias, R. Khare, A. Malek and A. Bhan, *J. Catal.*, 2013, **303**, 135–140.
23 Ch. Baerlocher, L. B. McCusker and D. H. Olson, *Atlas of Zeolites Framework Types*, Elsevier, Amsterdam, 6th edn, 2007.
24 Z. M. Cui, Q. Liu, Z. Ma, S. W. Bian and W. G. Song, *J. Catal.*, 2008, **258**, 83–86.

25 K. K. Ramasamy and Y. Wang, *J. Energy Chem.*, 2013, **22**, 65–71.
26 M. W. Erichsen, S. Svelle and U. Olsbye, *J. Catal.*, 2013, **298**, 94–101.
27 W. Dai, G. Wu, L. Li, N. Guan and M. Hunger, *ACS Catal.*, 2013, **3**, 588–596.
28 Y. Ma, N. Li, X. Ren, S. Xiang and N. Guan, *J. Mol. Catal. A: Chem.*, 2006, **250**, 9–14.
29 P. Meriaudeau, V. A. Tuan, V. T. Nghiem, S. Y. Lai, L. N. Hung and C. Naccache, *J. Catal.*, 1997, **169**, 55–66.
30 A. Buchholz, W. Wang, M. Xu, A. Arnold and M. Hunger, *Microporous Mesoporous Mater.*, 2002, **56**, 267–278.
31 Y. Jiang, J. Huang, W. Dai and M. Hunger, *Solid State Nucl. Magn. Reson.*, 2011, **39**, 116–141.
32 N. Rahimi and R. Karimzadeh, *Appl. Catal., A*, 2011, **398**, 1–17.
33 A. J. Marchi and G. F. Froment, *Appl. Catal., A*, 1991, **71**, 139–152.
34 T. V. W. Janssens, S. Svelle and U. Olsbye, *J. Catal.*, 2013, **308**, 122–130.
35 Y. Jiang, J. Huang, V. R. R. Marthala, Y. Ooi, J. Weitkamp and M. Hunger, *Microporous Mesoporous Mater.*, 2007, **105**, 132–139.
36 W. Wang, Y. J. Jiang and M. Hunger, *Catal. Today*, 2006, **113**, 102–114.
37 J. W. Park and G. Seo, *Appl. Catal., A*, 2009, **356**, 180–188.
38 H. Binder, A. Anikin and B. Kohlstrunk, *J. Phys. Chem. B*, 1999, **103**, 450–460.
39 *H NMR Predictor, Product Version 9.08*, Advanced Chemistry Development Inc., 2006.
40 W. Dai, M. Scheibe, N. Guan, L. Li and M. Hunger, *ChemCatChem*, 2011, **3**, 1130–1133.
41 W. Dai, W. Kong, G. Wu, N. Li, L. Li and N. Guan, *Catal. Commun.*, 2011, **12**, 535–538.
42 C. M. Wang, Y. D. Wang and Z. K. Xie, *J. Catal.*, 2013, **301**, 8–19.

